Appl. Phys. B 73, 417–423 (2001)
DOI: 10.1007/s003400100690

Applied Physics B
Lasers and Optics

X. WANG
S. NEUKERMANS
F. VANHOUTTE
E. JANSSENS
G. VERSCHOREN
R.E. SILVERANS
P. LIEVENS✉

Stability patterns and ionization potentials of Cr_nO_m clusters ($n = 3-50,\ m = 0, 1, 2$)

Laboratorium voor Vaste-Stoffysica en Magnetisme, K.U. Leuven, Celestijnenlaan 200D, 3001 Leuven, Belgium

Received: 25 July 2001/Revised version: 21 August 2001
Published online: 10 October 2001 •

ABSTRACT Chromium and chromium oxide clusters (Cr_nO_m, $n = 3$–50, $m = 0, 1, 2$) were produced by a laser vaporization cluster source, and investigated by laser photoionization spectroscopy and photofragmentation spectroscopy in combination with mass spectrometry. Ionization potentials for Cr_nO_m clusters ($m = 1, 2$) deduced from photoionization spectroscopy measurements show a smoothly decreasing trend with size similar to the behavior of other transition metals. Superimposed on this is a diffuse step from 8 to 11 chromium atoms, possibly indicating a structural transition. Mass-abundance spectra recorded with low-fluence, high-photon-energy ionization (6.4 eV) reveal stability steps for Cr_nO_m clusters ($n = 3$–50, $m = 1, 2$), corresponding to icosahedral geometrical shell closings insensitive to the oxygen content. These magic numbers are also found for $Cr_nO_m^+$ clusters ($n = 3$–50, $m = 0, 1, 2$) investigated with photofragmentation.

PACS 36.40.Cg; 36.40.Mr; 36.40.Qv

1 Introduction

Since the observation of shell structure in the mass-abundance spectra of sodium clusters by Knight et al. in 1984 [1], research on metallic clusters has continued and diversified. At present, the electric properties and the geometric shapes and structures of several metal clusters have been thoroughly studied theoretically and experimentally [2, 3]. For simple metal clusters, plenty of experimental observations show pronounced features as a function of cluster size, which are often related to the electronic structures. Different models were developed to describe the fermion system in metallic clusters, mainly differing in their degree of sophistication. Shell-model approaches, such as the jellium model, consider valence electrons delocalized within a positively charged background region formed by the core ions, in this way filling electronic levels in a potential well. In mass-abundance spectra representing ensembles of clusters in thermal equilibrium, high cluster stability will show up as a relatively enhanced abundance for these clusters. For simple metals, such as alkali metals or coinage metals, these enhanced stabilities occur for clusters with a number of delocalized electrons corresponding to a closed shell.

✉ Fax: +32-16/32-7983, E-mail:peter.lievens@fys.kuleuven.ac.be

Although such shell models provide a useful way to understand the electronic structure of the clusters of some main-group metals, they become not only complex but also inadequate for the description of non-coinage, transition-metal clusters. The unfilled d shell of these transition metals, as well as an anticipated size-dependent number of delocalized electrons, makes elaborate theoretical research much more complicated.

Alternatively, enhanced stability can be induced by specific compact ionic geometries, where stable structures emerge for a number of atoms corresponding to a closed shell of atoms [4]. In this case, experimentally observed enhanced abundances signal cluster stability related to the closing of a shell of atoms, defined as a structure with just enough atoms added to a previous shell as needed to regain the original symmetry. For example, the systematic adding of atoms to the faces of a tetrahedral structure reconstructs the original symmetry for each completed face, a total of four geometric shells for a complete layer of atoms [4].

Of the several kinds of geometric forms considered for free clusters, the icosahedral structure has the highest symmetry [4]. Each of the 20 triangular faces of an icosahedron can be constructed with close-packed spheres. However, this structure is highly strained: it cannot grow into a bulk structure and is found to be favorable only for clusters with a high surface-to-volume ratio. In spite of this limitation, icosahedral and subicosahedral structures are preferential structures for many cluster species and can often explain the stability patterns of these clusters.

Among the $3d$ transition metals, chromium is peculiar because of its electronic configuration: both its outer $3d$ and $4s$ shells are half filled. This results in a highly stable dimer structure with a very short bond length. Chromium dimers have been investigated thoroughly, as were several small oxygen-rich chromium oxide molecules [5–7]. Ionization and fragmentation studies of large oxygen-rich chromium clusters have been carried out by mass spectrometry [8]. Moreover, theoretical work on the structure and the electronic properties of small chromium-rich oxides and pure chromium clusters was reported [9, 10]. Nevertheless, very little experimental information is available and so far is restricted to photoelectron spectroscopy investigations of Cr_n ($n = 2$–70) [11].

In this paper we present the production and mass spectrometric investigation of chromium and chromium oxide clusters Cr_nO_m ($n = 3$–50, $m = 0, 1, 2$). Ionization potentials

(IPs) of Cr_nO and Cr_nO_2 clusters deduced from threshold photoionization spectroscopy measurements are presented. Time-of-flight mass spectra recorded after low-photon-fluence ionization (photoionization) and high-photon-fluence ionization (photofragmentation) of the produced clusters resulted in mass-abundance spectra showing evidence for icosahedral magic numbers. The results will be discussed with respect to existing theoretical studies, and compared to similar experimental data for other transition-metal clusters.

2 Production and mass spectrometry

The chromium clusters are produced using a home-built laser vaporization source. A review of this source can be found in [12]. Here only a brief description of the source and cluster-production process is given. A rectangular target of the desired material is moved in a closed-loop pattern under computer control and exposed to the focussed laser light of a pulsed Nd:YAG laser (Spectra Physics GCR-11, 532 nm, 10 Hz). Synchronous with the ablation of the target surface, helium gas is injected into the source by a pulsed gas valve (R.M. Jordan Co., Pulsed Supersonic Valve, 10 Hz), typically with a pressure of 7 bar. Cluster formation is initiated by collisions between atoms and clusters of the vaporized material and inert-gas atoms. This mixture of atoms, clusters and inert gas undergoes a supersonic expansion into a vacuum chamber (1×10^4 mbar) through a nozzle. For the presented work, a conical nozzle was used of 1.2 mm diameter and 10° opening angle. The isentropic expansion reduces the temperature of the cluster beam and because of the rapidly decreasing density, ends the cluster-growth process. In this way, a free molecular beam of clusters with an estimated temperature at or below room temperature is obtained.

The cluster beam passes a stainless-steel skimmer to remove extraneous helium gas. The homogeneous central part of the beam then enters the acceleration zone of a reflectron time-of-flight mass spectrometer (RTOF-MS) ($M/\Delta M \approx 1000$ amu at $M = 100$). In this study, both ionic and neutral clusters were produced and investigated by mass spectrometry. Cationic clusters are accelerated by a pulsed homogeneous field applied to the extraction electrodes and detected after their flight through the field-free region of the RTOF-MS.

In order to investigate neutral clusters, ionic clusters are eliminated from the beam by electrostatic deflection before entering the mass spectrometer. In the extraction region neutral clusters are ionized by laser light, accelerated by the pulsed electrostatic field and mass selected in the RTOF-MS. The photon fluence is kept low enough in order to prevent multi-photon absorption processes. In the remainder of the text, the neutrally produced clusters are referred to as *photoionized* clusters, while the ionically produced clusters under investigation are referred to as *cationic* clusters.

Figure 1 shows the low-mass part of a mass-abundance spectrum as typically obtained for cationic clusters (a) and photoionized clusters (6.43 eV) (b). In both cases the most abundant peaks are followed by one or two satellite peaks. For the cationic clusters, the most abundant species are pure chromium clusters Cr_n^+ with Cr_nO^+ and $Cr_nO_2^+$ as less abundant satellites. However, for photoionized clusters the most abundant species are the chromium monoxide Cr_nO clusters with intense Cr_nO_2 satellites.

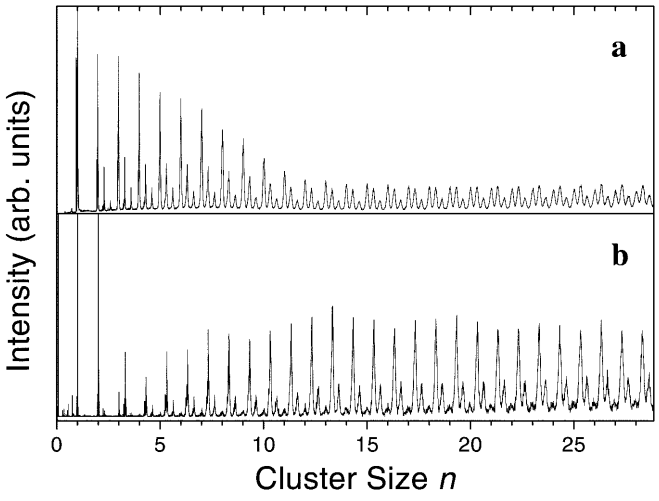

FIGURE 1 Mass spectra of cationic $Cr_nO_m^+$ (**a**) and photoionized Cr_nO_m clusters (**b**). The most abundant cationic species are Cr_n^+, contrary to the photoionized clusters where Cr_nO clusters dominate the spectrum

Not surprisingly, the high reactivity of chromium leads to oxygen contamination. The oxygen atoms may stem from impurities in the He gas and/or surface oxidization of the chromium-metal target. This contamination is reduced due to the precautions taken in the production procedure: before starting chromium-cluster production, the cluster source is thoroughly cleaned, the target is cleaned by laser sputtering and high purity helium gas (N60) is employed. As a result, only suboxide clusters with a few oxygen atoms are detected.

The difference in the relative abundances of the observed photoionized and cationic cluster species is striking: while a significant amount of cationic, pure chromium clusters Cr_n^+ is produced, the abundance of Cr_n is very low in the photoionized mass spectrum, apart from the atom, dimer and trimer. The reason for this difference between cluster charge states is not completely clear. However, it is possibly linked to the reduced stability of the neutral trimer Cr_3 caused by its particular structure: an essentially unaltered strongly bound dimer together with a weakly attached monomer [10]. In comparison, the binding energy of Cr_3^+ with respect to decomposition into a dimer cation and a neutral atom was measured to be about 2 eV [13], which is substantially higher than that for the neutral Cr_3, about 1 eV [10]. Therefore, growth of neutral pure chromium clusters may be less efficient in comparison with the growth of pure chromium cluster cations and oxidized chromium clusters, which do not rely on the Cr_3 precursor.

3 Threshold photoionization spectroscopy

Threshold photoionization spectroscopy in combination with mass spectrometry is applied to measure the ionization potentials of the chromium clusters. Two laser systems are employed: a tunable optical parametric oscillator as scanning ionization laser (Spectra Physics MOPO with frequency-doubling option) and an ArF excimer laser with fixed wavelength as reference laser (Lambda Physik Compex 102, 193 nm).

The measurement procedure is extensively described in [14]. In short, mass-abundance spectra of photoionized Cr_nO_m ($n = 3$–50, $m = 1, 2$) clusters are recorded as a function of photon energy. The laser photon energy is scanned in steps of 0.04 eV ranging from 4.56 to 5.6 eV. To reduce the effects of short term production fluctuations, 5000 cluster-production cycles per photon energy are added to produce one mass spectrum. Long term drifts are eliminated by normalizing each obtained mass spectrum with simultaneously recorded photoionization spectra at the fixed reference photon energy of 6.43 eV. This was achieved by alternating the reference laser beam and the scanning ionization laser beam every 50 laser shots. Furthermore, laser pulse energies are carefully monitored and the wavelength dependent attenuation of the laser beams through the entrance windows of the vacuum chamber (UV-grade silica) is taken into account. For all measurements, the laser pulse energy is kept low enough to prevent multi-photon processes.

For sufficiently low photon energies, no clusters are ionized in the considered size range. As the photon energy increases, clusters with higher IPs gradually appear in the mass spectra, as is illustrated by Fig. 2. From the collected mass spectra the ion yield vs. photon energy is deduced for each cluster size. The resulting photoionization efficiency (PIE) curves give the ionization probability of a cluster with a certain size as a function of the photon energy. Some selected photoionization efficiency curves of Cr_nO clusters are shown in Fig. 3.

The ionization potentials are extracted from the PIE curves by linearly extrapolating the main post-threshold portion to the baseline of the signal. For several clusters, this procedure is not unique. As shown in Fig. 3, two distinct slopes can be clearly observed in the PIE curves for the smaller clusters. This can be attributed to several causes: inhibited ionization to the ionic ground state because of the Franck–Condon effect, the presence of isomers, thermal excitations of the neutral clusters or cation production by multi-photon ionization or fragmentation of larger sizes. The existence of several low lying isomers for chromium clusters has indeed been predicted [9, 10]. Due to the rapid cooling of the clusters in the expansion process, initially populated isomeric states may survive in the beam. This cooling mechanism should reduce the presence of thermal tails attributable to vibrational hot bands. Although great care has been taken to prevent multi-photon absorption, photofragmentation, especially of very large clusters, cannot be completely excluded.

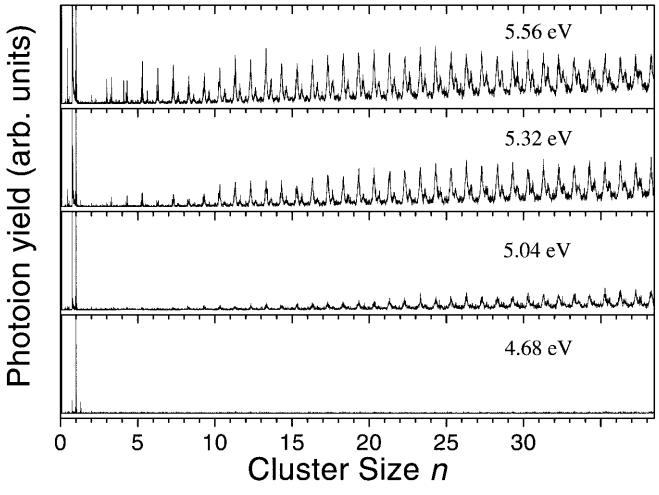

FIGURE 2 Mass-abundance spectra of Cr_nO_m clusters ionized with different photon energies

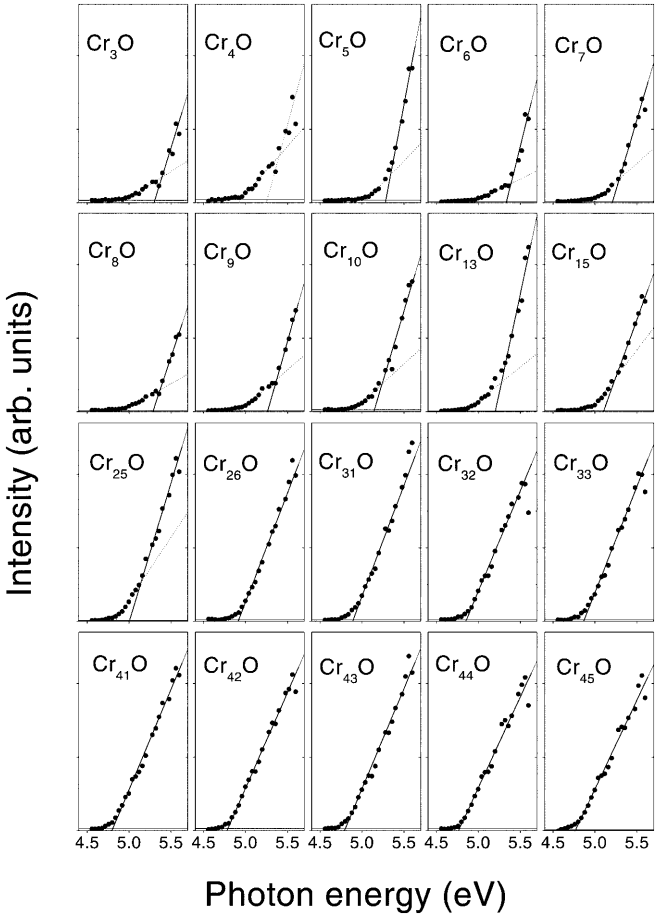

FIGURE 3 Photoionization efficiency curves for selected chromium monoxide clusters

In the work presented here, the ionization potentials were systematically assigned by using the most prominent slope of the PIE curves. The extracted values for the chromium oxide clusters are listed in Table 1. The uncertainties in the evaluation procedure to extract these values are taken into account by $\pm$ 0.05 eV error limits. The relation between these ionization-energy values and the cluster sizes is shown in Fig. 4.

Earlier observation of odd–even staggering effects in the electron affinities of small chromium clusters were interpreted as evidence for dimerization (from $n = 3$–8) of the cluster geometric structure [11]. Although in our measured values for the ionization energy of Cr_nO clusters odd–even staggering effects are to some extent present, e.g. for $n = 5$–8, this phenomenon is not obvious and a similar interpretation is not straightforward here.

The general evolution of the IPs with size shows two main features: after nearly constant values for the lower sizes, a clear drop from $n = 8$ to $n = 11$ can be noticed both for the Cr_nO and the Cr_nO_2 clusters. The reason for this diffuse step at $n = 8$–11 is not clear. One can speculate that the

n	IP of Cr_nO (eV)	IP of Cr_nO_2 (eV)
4	(5.26)	5.25
5	5.26	5.29
6	5.34	5.30
7	5.21	5.28
8	5.29	5.30
9	5.27	5.25
10	5.14	5.19
11	5.05	5.14
12	5.10	5.18
13	5.20	5.10
14	5.08	5.12
15	5.10	5.10
16	5.04	5.12
17	5.03	5.06
18	5.07	5.06
19	5.02	5.08
20	4.99	5.05
21	4.99	5.03
22	5.00	5.01
23	4.98	5.03
24	4.98	4.98
25	5.00	4.96
26	4.92	4.96
27	4.88	4.97
28	4.93	4.90
29	4.89	4.96
30	4.90	4.90
31	4.89	4.90
32	4.86	4.95
33	4.86	4.88
34	4.86	4.88
35	4.84	4.88
36	4.84	4.85
37	4.82	4.83
38	4.82	4.80
39	4.80	4.82
40	4.80	4.84
41	4.80	4.80
42	4.79	4.80
43	4.80	4.80
44	4.78	4.81
45	4.77	4.80
46	4.79	4.79
47	4.78	4.78
48	4.77	4.77
49	4.78	4.77
50	4.76	4.75

TABLE 1 Ionization potentials (± 0.05 eV) of Cr_nO_m clusters ($n = 3$–50, $m = 1, 2$)

drop reflects a change of cluster-growth mechanisms, from dimerized structures for the very small sizes where the strong chromium dimer bonding is playing an essential role, towards more frequently encountered close-packing structures as proposed for other transition-metal clusters [10]. Alternatively, this drop of ionization energy could be related to the change of geometric structures from clusters with all atoms on the surface, to clusters with one or more interior atoms [15].

Moreover, the IPs of Cr_nO_m ($m = 1, 2$) clusters do not exhibit the dramatic discontinuities as displayed by clusters of the nearly-free-electron metals such as alkali metals. This lack of shell behavior is a general feature of transition-metal clusters due to the involvement of d electrons in the cluster bonding. Additionally, some influence of different geometric isomers with different IPs cannot be completely excluded.

Figure 4 shows a comparison between the ionization potentials of the monoxide and the dioxide clusters. Both show

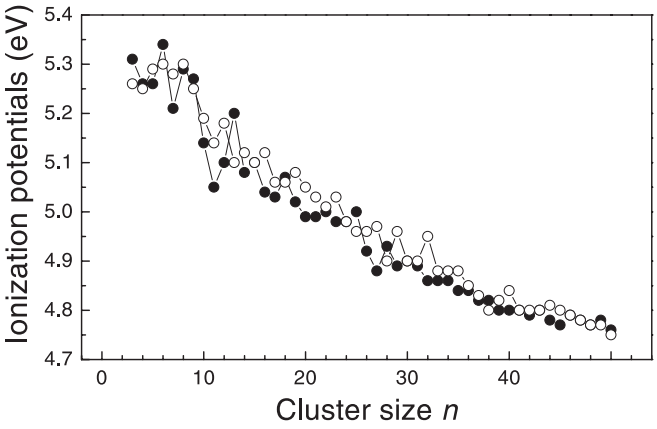

FIGURE 4 Ionization potentials of chromium monoxide (•) and dioxide (○) clusters as a function of cluster size n

very similar values for the ionization potentials for the same number of chromium atoms. Observed differences in the odd–even staggering are within the error margins. This similarity indicates that for chromium-rich clusters the influence of oxygen atoms on the electronic properties is limited. For underdoped metallic clusters, in which the metallic part is much greater, the presence of an electronegative impurity is fully screened by the valence electrons. Consequently the metallic characteristics of these doped clusters tend to be similar to those of the pure metallic clusters [16, 17]. This trend differs from the observations for oxidized alkali clusters (see e.g. [14, 18]), where each electronegative oxygen atom tends to localize two valence electrons.

Traditionally, the ionization potentials of metallic clusters as a function of radius can be compared with predictions in a classical spherical droplet (CSD) model picture:

$$IP = WF + \frac{\alpha e^2}{R},$$

where R is the cluster radius, WF is here the work function of bulk chromium (4.5 eV) and the classical value for α is $1/2$. Since it can be expected that, at least for the larger sizes, the oxygen atoms alter neither the geometry nor the IPs significantly, R was estimated from theoretical calculations of the geometry of pure chromium clusters [10].

Figure 5 shows the comparison between experimental results and the CSD model. Similar to the results of nickel, iron and cobalt clusters [19, 20], a large deviation is observed, which indicates that this classical model is not suitable to predict the ionization potentials of transition-metal clusters. However, if we use a reduced work function ($WF_{\mathrm{Cr\ reduced}} = 4.5 - 0.95 = 3.55$ eV), the results for large clusters are consistent with this model for α equal to $3/8$. This behavior was also found for other transition-metal clusters (WF_{Ni} was reduced by 0.46 eV, WF_{Fe} by 0.3 eV and WF_{Co} by 0.5 eV) [19, 20] and oxide clusters such as Sc_nO [21]. The limitations of the CSD model for transition-metal clusters in this size domain can be attributed to several reasons. The surface atoms play an important role in determining the work function, which could lead to a different work function for clusters and bulk matter. Additionally, the electronic structure of a cluster can be sufficiently different from bulk to give rise to a deviation from the CSD model.

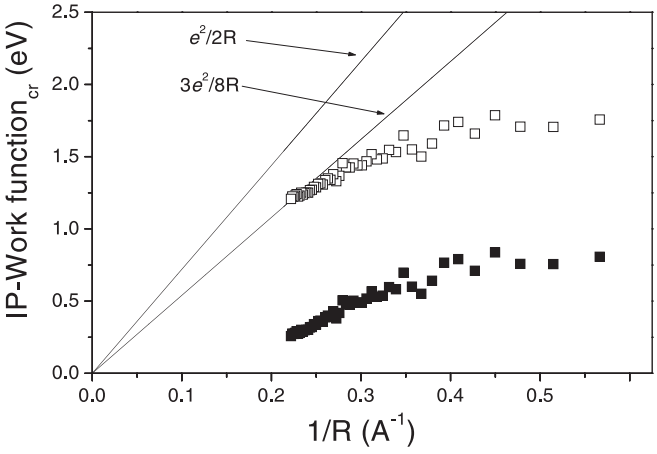

FIGURE 5 Comparison of measured Cr_nO ionization potentials with the predictions of the CSD model for two assumed values of the bulk work function (for *solid squares*: $WF = 4.5$ eV; for *open squares*: $WF = 3.55$ eV)

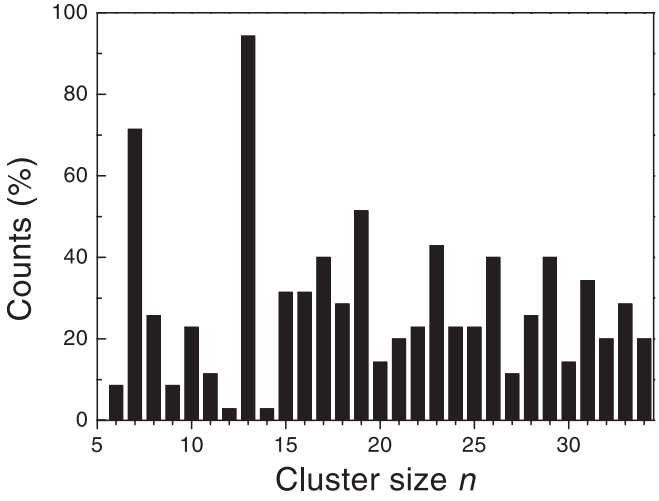

FIGURE 6 Appearance of enhanced relative abundances for Cr_nO clusters in mass spectra recorded with low-fluence, high photon energy (6.43 eV)

4 Evidence for geometric stability effects

4.1 *Stability patterns in production spectra*

Mass-abundance measurements of clusters are regularly used to determine mass-dependent stability features, but the appearance of steps in abundance spectra crucially depends on details of the production method. In this respect, laser vaporization sources are known not to show many stability features, because of the non-equilibrium production conditions [3]. Nevertheless, a careful analysis of the mass spectra does show some stability effects. Slightly higher mass peaks with respect to neighboring masses can be observed for 7 and 13 chromium atom clusters, as is indicated in Fig. 1b. This figure corresponds to one of the reference measurements (photoionized by an excimer laser, 6.43 eV) recorded during the ionization-potential measurements (see above). In order to confirm these (and other) abundance features, a statistical analysis of the photoionization reference mass abundance spectra was performed. For each independent measurement (in total nearly 100 mass spectra or 500 000 production cycles), the peaks that are higher with respect to the neighboring masses are counted. The frequency of being counted as a local maximum is plotted for Cr_nO ($6 \leq n \leq 34$) in Fig. 6. In this plot the relative abundance enhancement is extremely pronounced for $n = 7$ and 13 and also quite clear for $n = 19$, 23, 26 and 29.

Since the spectra used for this evaluation are obtained by low-fluence photoionization, it is not clear a priori whether or not the observed features are due to size dependent ionization efficiencies. However, as was discussed above, only a smooth size dependence of the IPs is observed and the IPs are all well below 6.43 eV. Therefore, it appears justified to relate the abundance enhancements to a larger production probability, which is genuinely believed to be associated with an enhanced relative stability. We conclude that Cr_nO clusters with 7, 13, 19, 23, 26 or 29 chromium atoms are more stable with respect to their neighbors, and these sizes can be referred to as magic numbers. Due to the much lower production rate, a similar analysis on Cr_nO_2 clusters is less reliable. In spite of this, evidence for a higher stability for very similar numbers, $n = 6$, 13, 19 and 23, could be deduced from the mass spectra following a similar procedure.

For several transition-metal clusters (e.g. iron, titanium and zirconium) [22], comparable magic numbers have been related to the occurrence of shells of geometric structure. Here an icosahedral structure can be used to explain our observations. $n = 13$ corresponds to a centered single-shell icosahedral structure (Fig. 7b); $n = 19$ is a double icosahedron (Fig. 7c). Likewise the occurrence of stable clusters with 23 and 29 metal atoms can be explained as icosahedral subshells. For $n = 7$, a half-icosahedral structure (Fig. 7a) can be proposed although pure chromium clusters were calculated to have a dimer-based structure consisting of three dimers plus an extra atom (Fig. 7d) [10]. However, for a small cluster like

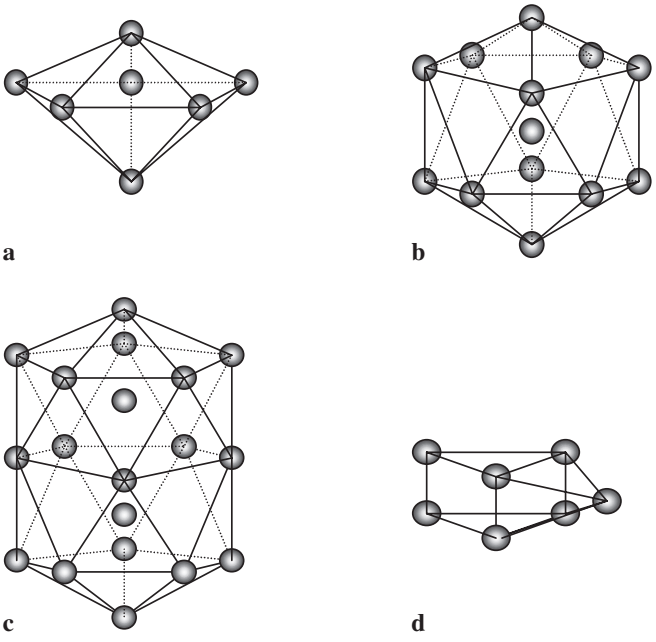

FIGURE 7 Suggested stable geometric structures. Half-icosahedral structure for $n = 7$ (**a**); icosahedron for $n = 13$ (**b**); double icosahedron for $n = 19$ (**c**) and structure calculated for Cr_7 [10] (**d**)

Cr_7O, the influence of the oxygen atom may be significant enough to alter the structure.

Another feature attributed to many transition metals is an enhanced stability at 15 cluster atoms, corresponding to a *bcc* structure [9, 10, 22]. This is not immediately apparent in our analogous case of $Cr_{15}O$.

The fact that for both monoxide and dioxide clusters largely the same numbers are observed indicates a weak influence of oxygen doping on the cluster geometry, and occurs if the oxygen atom would be incorporated in one of the tetrahedral building blocks of the icosahedral structures. Similar observations, calculations and interpretations were reported previously for other metal clusters, e.g. for metal rich Ba oxides [23, 24]. So far no structure calculations exist for small chromium suboxide clusters.

4.2 *Photofragmentation spectroscopy*

An alternative way to deduce information concerning the stability of clusters as a function of size is to induce cluster excitation and subsequent cluster decay into fragments. In our case, excitation relies on multi-photon absorption followed by ionization and fragmentation, mainly by evaporation of monomers or dimers [3]. This technique has already been used in studies of electronic shell structures in bimetallic clusters. Details of the experimental procedure can be found in [25]. In brief, high-fluence ArF laser light irradiates the neutral cluster beam, and photofragments are detected by time-of-flight mass spectrometry. Photofragments with relatively high stability are highlighted by enhanced abundances in the mass spectra.

The resulting mass-abundance plot for chromium clusters is shown in Fig. 8. Abundance steps at several cluster sizes are clearly visible, indicated in the insert of Fig. 8 for the pure Cr_n^+ and for the oxidized Cr_nO^+ and $Cr_nO_2^+$ photofragments. Most pronounced are the steps at $n = 7$, 13, 19, 23, 26 and 29 for the monoxides and at $n = 13$ and 19 for the dioxides, confirming the findings of the mass-abundance analysis discussed above.

Less structure is visible for the Cr_n^+ photofragments although our studies reveal indications of systematic, weak steps at $n = 14$, 20 and 24. This apparent shift of the most stable sizes with one atom is consistent with binding energies deduced from collision-induced dissociation experiments of Cr_n^+ with Xe [13]. This shift can be explained as in cationic noble-gas clusters with the dimeric core model giving distorted icosahedral and double icosahedral structures with the central atom replaced by a dimer [26]. Interestingly, this model implies an icosahedral structure for the neutral Cr_n clusters.

The icosahedral structure of Cr_nO_m and $Cr_nO_m^+$ for values of n equal to or larger than seven can be correlated to the diffuse step found in the ionization potentials. This step may now be explained as due to transition from the growth of small chromium clusters to icosahedral growth for larger clusters.

5 Summary and conclusion

Chromium-rich Cr_nO_m clusters are produced in a laser vaporization source. Neutral and cationic clusters show different cluster-species abundances, with Cr_n clusters being almost absent, contrary to the strong presence of Cr_n^+. This can be tentatively explained by the low stability of the Cr_3 precursor compared to Cr_3^+ or the chromium oxides.

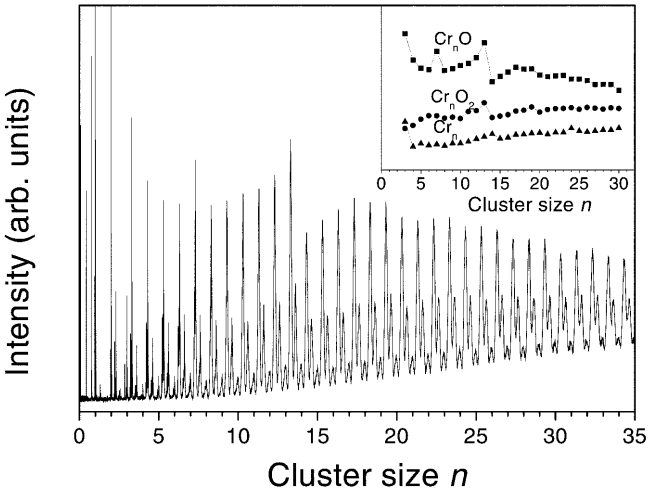

FIGURE 8 Photofragmentation stability patterns for chromium and chromium oxide cluster cations. *Insert* shows the height of the mass peaks corresponding to Cr_n^+, Cr_nO^+ and $Cr_nO_2^+$ photofragments

Identical magic numbers n corresponding to icosahedral shell closings can be found for Cr_nO_m and $Cr_nO_m^+$, for both oxidized species under consideration. This indicates a general insensitivity of the geometric structure to the actual oxygen content for all but the smallest clusters in the underdoped regime. In addition, evidence was found for distorted, dimer-core icosahedral structures for the Cr_n^+ photofragments. These observations serve as strong indications that larger Cr_n clusters have an icosahedral structure, deviating from the dimer-based growth mechanism calculated for smaller sizes.

It is possible that a similar structural transition results in the diffuse step observed at $n = 8$–11 in the ionization potentials of the chromium oxide clusters. This step is superimposed on the smoothly decreasing behavior with size expected for the ionization potential of a transition-metal cluster. Furthermore, no systematic difference was measured between the ionization potentials of Cr_nO and Cr_nO_2 clusters, revealing that the oxygen atoms do not strongly influence the electronic structure either.

ACKNOWLEDGEMENTS This work has been financially supported by the Fund for Scientific Research – Flanders (F.W.O.), by the Flemish Concerted Action (G.O.A.) Research Program and by the Belgian Interuniversity Poles of Attraction Programme (I.U.A.P.), Belgian State, Prime Minister's Office, Federal Office for Scientific, Technical and Cultural Affairs. S.N. and E.J. are Research Assistants of the F.W.O.

REFERENCES

1 W.D. Knight, K. Clemenger, W.A. de Heer, W.A. Saunders, M.Y. Chou, M.L. Cohen: Phys. Rev. Lett. **52**, 2141 (1984)
2 M. Brack: Rev. Mod. Phys. **65**, 677 (1993)
3 W.A. de Heer: Rev. Mod. Phys. **65**, 611 (1993)
4 T.P. Martin: Phys. Rep. **273**, 199 (1996)
5 G.V. Chertihin, W.D. Bare, L. Andrews: J. Chem. Phys. **107**, 2798 (1997)
6 S. Veliah, K.H. Xiang, R. Pandey, J.M. Recio, J.M. Newsam: J. Phys. Chem. B **102**, 1126 (1998)
7 B.V. Reddy, S.N. Khanna: Phys. Rev. Lett. **83**, 3170 (1999)

8 G.C. Nieman, E.K. Parks, S.C. Richtsmeier, K. Liu, L.G. Pobo, S.J. Riley: High Temp. Sci. **22**, 115 (1986)
9 B.V. Reddy, S.N. Khanna, P. Jena: Phys. Rev. B **60**, 15 597 (1999)
10 H.S. Cheng, L.S. Wang: Phys. Rev. Lett. **77**, 51 (1996)
11 L.S. Wang, H.B. Wu, H.S. Cheng: Phys. Rev. B **55**, 12 884 (1997)
12 W. Bouwen, P. Thoen, F. Vanhoutte, S. Bouckaert, F. Despa, H. Weidele, R.E. Silverans: Rev. Sci. Instrum. **71**, 54 (1999)
13 C.-X. Su, P.B. Armentrout: J. Chem. Phys. **99**, 6506 (1993)
14 P. Lievens, P. Thoen, S. Bouckaert, W. Bouwen, F. Vanhoutte, H. Weidele, R.E. Silverans: J. Chem. Phys. **110**, 10 316 (1999)
15 K. Athanassenas, D. Kreisle, B.A. Collings, D.M. Rayner, P.A. Hackett: Chem. Phys. Lett. **213**, 105 (1993)
16 F. Despa, W. Bouwen, F. Vanhoutte, P. Lievens, R.E. Silverans: Eur. Phys. J. D **11**, 403 (2000)
17 F. Despa: Phys. Lett. A **276**, 109 (2000)
18 T. Bergmann, H. Limberger, T.P. Martin: Phys. Rev. Lett. **60**, 1767 (1988)
19 M.B. Knickelbein, S. Yang, S.J. Riley: J. Chem. Phys. **93**, 94 (1990)
20 S. Yang, M.B. Knickelbein: J. Chem. Phys. **93**, 1533 (1990)
21 S. Yang, M.B. Knickelbein: Z. Phys. D **31**, 199 (1994)
22 M. Sakurai, K. Watanabe, K. Sumiyama, K. Suzuki: J. Chem. Phys. **111**, 235 (1999)
23 V. Boutou, M.A. Lebeault, A.R. Allouche, F. Paulig, J. Viallon, C. Bordas: J. Chem. Phys. **112**, 6228 (2000)
24 V. Boutou, M.A. Lebeault, A.R. Allouche, C. Bordas, F. Paulig, J. Viallon, J. Chevaleyre: Phys. Rev. Lett. **80**, 2817 (1997)
25 W. Bouwen, F. Vanhoutte, F. Despa, S. Bouckaert, S. Neukermans, L. Theil Kuhn, H. Weidele, P. Lievens, R.E. Silverans: Chem. Phys. Lett. **314**, 227 (1999)
26 H.-U. Böhmer, S.D. Peyerimhoff: Z. Phys. D **11**, 239 (1989)